Applied Catalysis B: Environmental 306 (2022) 121138

Contents lists available at ScienceDirect

Applied Catalysis B: Environmental

journal homepage: www.elsevier.com/locate/apcatb

Promoting catalytic transfer hydrodecarbonylation of methyl stearate over bimetallic CoNi/HAP catalysts with strong electronic coupling effect

Hao Yan [a], Shuang Yao [a], Tong Zhang [a], Delong Li [a], Xiaoyu Tang [a], Mengxin Chen [a], Yixuan Zhou [a], Mingrui Zhang [b], Yibin Liu [a,*], Xin Zhou [a], Xiang Feng [a], Xiaobo Chen [a], Chaohe Yang [a]

[a] State Key Laboratory of Heavy Oil Processing, China University of Petroleum, Qingdao 266580, China
[b] Fushun Petrochemical Company Catalyst Plant, Fushun 113000, China

ARTICLE INFO

Keywords:
Hydrodecarbonylation
Methyl stearate
Non-noble metal catalyst
Heptadecane

ABSTRACT

Tailoring the hydrodeoxygenation capacity via the regulation of the electronic structure of the active site is still a significant challenge for hydrogenation of oxygenated substrates. Herein, we report the highly efficient bimetallic CoNi/HAP catalysts to promote the catalytic transfer hydrodecarbonylation of methyl stearate to heptadecane. Multiple characterizations reveal that the CoNi alloy nanoparticles with fcc structure exhibit strong electron coupling effect and enhanced adsorption of methyl stearate, leading to the improvement of catalytic activity. Specifically, the introduction of Ni changes the reaction pathway from methyl stearate → octadecanol over the Co/HAP catalyst to methyl stearate → heptadecane over CoNi/HAP catalysts. In situ Fourier transform infrared spectra, reaction kinetics and density functional theory calculation show that the heptadecane is mainly generated through hydrodecarbonylation (-CO) rather than hydrodecarboxylation (-COO) because the C—C bond cleavage of oxygenated intermediate (RCH_2CO) is greatly facilitated over the Ni active site of electron reconstructed CoNi alloy nanoparticles. Finally, the Co_5Ni_5/HAP catalyst exhibits excellent conversion (99.4%), heptadecane selectivity (98.2%) and catalyst stability. These insights revealed here could pave the way for the rational development of catalyst with high catalytic performance in the catalytic transfer hydrogenation system of fatty acids/esters.

1. Introduction

Renewable fatty acid methyl esters derived from the esterification of natural oils (microalgae oil, animal and vegetable oils) or waste cooking oils with methanol are promising for traditional fuel (long-chain alkanes) and valuable chemical production (high-ranking fatty alcohols) [1–9]. In particular, fuel-range hydrocarbon has been regarded as the most promising alternative to fossil fuels due to its high energy density and storage stability and low specific gravity [10,11]. Removing oxygen atoms from the fatty acid and its methyl esters is undoubtedly crucial for the production of hydrocarbons. However, this hydrodeoxygenation (HDO) process commonly requires high H_2 pressure, inevitably bringing safety difficulties in transportation and storage [12,13]. Moreover, considering that H_2 is still mainly obtained from fossil fuels in industry, the use of energy-intensive H_2 results in the HDO process expensive and unsustainable [14]. In this scenario, catalytic transfer hydrogenation of bio-based alcohols and water for renewable H_2 exhibits both economic and technological advantages in HDO.

Rational design of efficient HDO catalyst is the key to the catalytic transfer hydrogenation of fatty acid and its methyl esters to long chain alkanes. Generally, both noble metal (Pd, Pt and Ru) and non-noble metal catalysts (Ni, Cu, W, Mo, Co and Fe) have been widely employed in this process [15–22]. For example, Vardon et al. [23] achieved 100% conversion of oleic acid and 45.0% selectivity of heptadecane at 300 °C and 9 h over Pt-Re/AC catalyst using glycerol and water as hydrogen donors. Chen et al. [19] reported that stearic acid could be completely converted at 300 °C and 6 h over Ni/ZrO_2 catalyst with the introduction of H_2O as hydrogen donor, and the selectivity of heptadecane was around 31.0%. Fu et al. [11] and Nie et al. [10] both discovered that bimetallic CuNi catalysts display > 99% conversion and > 85% n-heptadecane selectivity for the catalytic transfer hydrogenation of oleic acid in the methanol-water/isopropanol system. Notably,

* Corresponding author.
E-mail address: liuyibin@upc.edu.cn (Y. Liu).

https://doi.org/10.1016/j.apcatb.2022.121138
Received 18 October 2021; Received in revised form 9 January 2022; Accepted 21 January 2022
Available online 25 January 2022

although noble metal catalysts show high hydrogenation activity, the selectivity of fatty alcohols or n-alkanes is limited due to the stronger adsorption of alcohols/H_2O on metal surface in the catalytic transfer hydrogenation system, resulting in the low n-alkanes selectivity [7,24]. In addition, the finite reserves and high cost of noble metal also strongly restrict their extensive application. Replacing noble metal catalysts with non-noble metal catalysts is the necessary way to realize the industrialization of HDO process. Unfortunately, up to date, there are few number of robust non-noble metal catalysts exhibiting superior catalytic performance (heptadecane yield > 95%) using cheap hydrogen donors (methanol and water) under mild reaction conditions (< 300 °C). Therefore, further developing high efficient and stable non-noble metal catalysts is highly desirable for the catalytic transfer hydrogenation of fatty acid and its methyl esters to long chain alkanes.

Recently, Co-based catalysts are demonstrated to display high activity toward C—O bond activation in the catalytic transfer hydrogenation of fatty acid and its methyl esters [10,12,14,25]. Furthermore, compared with other kinds of non-noble metal (especially Cu) catalysts, Co-based catalysts exhibit high resistance to deactivation in the presence of H_2O/alcohols (such as isopropanol and methanol) [12,14]. Recent studies have reported that a complete conversion of fatty acids with over 70% fatty alcohols selectivity could be obtained over stable Co-based catalyst using isopropanol/methanol and H_2O as a hydrogen donor [12,14]. Nevertheless, the selectivity of n-alkanes is quite low due to the poor hydrodeoxygenation ability of monometallic Co active sites. It is worth mentioning that Ni metal has already been proved to process strong C-O and C—C bonds activation ability in the hydrogenation of fatty acids and methyl esters [10,11,21,24]. On this foundation, the introduction of Ni into Co is expected to enhance the deoxygenation ability of methyl stearate catalytic transfer hydrogenation, promoting the formation of n-alkanes over the stable bimetallic CoNi catalysts.

In this work, the bimetallic CoNi/HAP catalysts are prepared for the catalytic transfer hydrogenation of methyl stearate to heptadecane. The underlying structure-performance relationship is systematically revealed by multiple characterizations. The results show that the introduction of Ni enhances the electron coupling effect of CoNi alloy nanoparticles and promotes the adsorption of methyl stearate, thus improving the catalytic activity. Meanwhile, the reaction pathway of catalytic transfer hydrogenation of methyl stearate to heptadecane is greatly promoted over the CoNi alloy nanoparticle. It is found that Co metal active site promotes the formation of oxygen-containing intermediates before octadecanol, and the Ni active site induces the cleavage of C—C bond of RCH_2CO intermediate (hydrodecarbonylation), resulting in the high heptadecane selectivity. The methodology and insights in this work could lay some foundations for the rational design and engineering of catalysts in the catalytic transfer hydrogenation system of renewable fatty acids/esters.

2. Experimental

2.1. Chemicals

Calcium nitrate tetrahydrate ($Ca(NO_3)_2{\cdot}4H_2O$, 99%), ammonium dihydrogen phosphate ($NH_4H_2PO_4$, 99%), ammonia solution tetrahydrate ($NH_3{\cdot}H_2O$, 25–28%), cobalt nitrate hexahydrate ($Co(NO_3)_2{\cdot}6H_2O$, 99%), activated charcoal (CP, 200 mesh), silicon dioxide (SiO_2, 99.5%, 30 nm), nickel(II) nitrate hexahydrate ($Ni(NO_3)_2{\cdot}6H_2O$, 99%) and methanol (CH_3OH, 99%) were purchased from Sinopharm Chemical Reagent Co., Ltd. Methyl stearate ($C_{19}H_{38}O_2$), n-alkanes (heptadecane and octadecane) and stearic acid ($C_{18}H_{36}O_2$) were provided by Sigma-Aldrich.

2.2. Catalyst preparation

The detailed preparation process of hydroxyapatite (HAP) has been described in our previous work [12]. In brief, a certain amount of CTAB and $Ca(NO_3)_2{\cdot}4H_2O$ solutions were dropped into the $NH_4H_2PO_4$ solution at 80 °C. After stirred for 2 h, the above mixture was transferred into the autoclave and hydrothermally treated at 110 °C for 24 h. After centrifugation, drying and calcination, HAP sample was obtained. All the bimetallic CoNi/HAP catalysts were prepared by incipient wetness impregnation method with deionized water as the solvent. The total theoretical metal loading was 10 wt% (based on mass). According to the different metal loading of Co and Ni, the catalysts were marked as Co/HAP, Co_8Ni_2/HAP, Co_5Ni_5/HAP, Co_2Ni_8/HAP and Ni/HAP. The Co_5Ni_5/AC (AC refers to activated carbon) and Co_5Ni_5/SiO_2 catalysts with the same metal loading and proportion as the Co_5Ni_5/HAP catalyst were also prepared by incipient wetness impregnation method.

2.3. Catalyst characterization

The specific surface area of these samples was measured by N_2-adsorption via Brunauer–Emmett–Teller (BET) method over Micromeritics ASAP 2020. Powder X-ray diffraction (XRD) was tested on the X′pert PRO MPD diffractometer with CuKα radiation. X-ray photoelectron spectroscopy (XPS) was tested on the Perkin-Elmer PHI ESCA device with an Al KR X-ray source. Transmission electron microscopy (TEM) was carried on the Tecnai G2 F20 S-Twin. Inductively coupled plasma optical emission spectrometry (ICP-OES) was tested on the VARIAN 720-ES (Table S1). In situ Fourier transform infrared spectra (in situ FT-IR) was performed on the Thermo Scientific Nicolet iS50. For in situ CO FT-IR, the catalysts were first pretreated at 300 °C for 1 h (40 mL/min, 10 vol% H_2 and Ar mixture gas). The CO adsorption was performed at 30 °C with the introduction of 5 vol% CO and Ar mixture gas. When CO adsorption was saturated, pure N_2 (40 mL/min) was blown into the in situ cell to remove the gas phase CO. All the spectra were collected using 32 scans with a resolution of 4 cm^{-1}. For in situ CO_2 FT-IR, the catalysts were also pretreated at 300 °C for 1 h (40 mL/min, 10 vol% H_2 and Ar mixture gas). The CO_2 adsorption was performed at 30 °C with the introduction of 5 vol% CO_2 and Ar mixture gas. When CO_2 adsorption was saturated, pure N_2 (40 mL/min) was blown into the in situ cell to remove the gas phase CO for 0.5 h. Temperature programmed reduction (TPR) and desorption (TPD) were tested on the Micromeritics AutoChem II 2920. For H_2-TPR, 0.1 g unreduced catalyst was pretreated at 300 °C for 1 h (40 mL/min, Ar). When the sample was cooled to 50 °C, the TCD signal was recorded under 10 vol% H_2 and Ar mixture gas (40 mL/min). For CO/CO_2-TPD, 0.1 g catalysts was pretreated at 300 °C for 1 h (40 mL/min, He). After the baseline was stabilized at 50 °C, 5 vol% CO_2/CO and Ar mixture gas was filled and adsorbed for 1 h. Then, the TCD signal was recorded from 50 °C to 700 °C (10 °C/min) under the flow of He (40 mL/min).

2.4. Catalytic test

In this paper, cheap methanol and H_2O were selected as the hydrogen donors. In order to be closer to the raw materials of animal and vegetable oils used in hydrogenation industry, methyl stearate (MS) instead of stearic acid (SA) was selected as a model compound to evaluate the catalytic performance. A large number of literature and our subsequent experiments have proved that methyl stearate and stearic acid can rapidly transform into each other in the presence of H_2O. Therefore, the catalytic transfer hydrogenation performance of methyl stearate and stearic acid over our Co_5Ni_5/HAP catalyst is almost the same. The evaluation experiments of the CoNi/HAP catalysts were carried out in the 50 mL high-pressure reactor. Typically, 20 mL deionized H_2O, 10 mL n-hexane, 3 mL methanol and 0.2 g catalyst were added into the reactor. Then it was sealed and purged with nitrogen at least three times to remove the internal air. When the reactor was heated to the set temperature, the stirring speed was raised from 100 rpm to 500 rpm. After the reaction, the gas products were analyzed by gas chromatography (GC) with the flame ionization detector (FID) and thermal conductivity detector (TCD). The liquid product was analyzed on the Scion 456-GC

equipped with an HP-5 column and an FID detector. When testing samples, eicosane was used as the internal standard. The definitions of conversion, selectivity and initial reaction rate have been described in our previous work [12].

2.5. Density functional theory (DFT) calculations

Density functional theory calculation was performed on the CASTEP module of Materials Studio 8.0 [26]. In the calculation process, generalized gradient approximation (GGA) with the Perdew–Burke–Ernzerhof (PBE) exchange-correlation functional was selected to describe the potential energy surface, and double numerical plus polarization (DNP) basis set were selected [27,28]. The vdW interaction was also corrected by TS's DFT-D2 method. The Monkhorst–Pack method was selected to sample 3 × 3 × 1 k-points, and the cutoff energy was set to 340 eV. A LST/QST method was used to find the transition state, and zero point energy correction was included in all the energies [29,30]. The maximum force field, stress and displacement for convergence were 0.05 eV/Å, 0.1 GPa and 0.002 Å, respectively. Because the supported Co nanoparticles were mainly exposed to (111) crystal plane, the (111) surface of the Co unit cell was cut to construct the Co(111) calculation model with a p(4 × 4) slab containing three layers with 12 atoms per layer in the 20 Å vacuum box [31–33]. Moreover, it is widely accepted that Co nanoparticles are easy to form fcc structure alloy nanoparticles with Ni and other metals when the reduction temperature is higher than 500 °C [34–39]. Therefore, for the CoNi(111) model, a periodic three-layer slab with sixteen Ni atoms per layer was first modeled representing a 4 × 4 unit cell and a vacuum of 20 Å in thickness. Then, according to the optimal Co_5Ni_5/HAP catalyst in the experiment, the Co atom was evenly substituted for the Ni atom in the molar ratio of 1:1 in the above model. In addition, the adsorption energy of propionic acid was calculated by the following formula: $E_{ads} = E_{PA/sub}-E_{PA}-E_{sub}$, where E_{sub}, E_{PA} and $E_{PA/sub}$ are the energy of calculation Co(111)/CoNi(111) model, the energy of propionic acid and the total energy of the calculation system, respectively.

3. Results and discussion

3.1. Promoting catalytic transfer hydrodeoxygenation of methyl stearate over bimetallic CoNi/HAP catalysts

Generally, the hydrogenation of methyl ester is a parallel sequential reaction (Fig. 1a). In the presence of H_2O, stearic acid (SA) is easily obtained by the hydrolysis of methyl stearate (MS) (Table S2). Subsequently, the stearic acid (SA) could be further hydrogenated to heptadecane (HP) or octadecanal (ODA). The as-formed ODA or its intermediates could be decarbonylated to heptadecane and hydrogenated to octadecanol (ODL), which can be further converted to octadecane (OD) [6,7]. Since methanol and water as hydrogen donors display the advantages of high atomic efficiency and low energy intensity (Table S3), we are interested in evaluating the catalytic performance of a series of bimetallic CoNi catalysts for the catalytic transfer hydrogenation of MS to HP. Fig. 1b shows that the initial reaction rate of the Co_5Ni_5/HAP catalyst (4.65 mmol/g_{metal}/h) is more than two times higher than that of the Co/HAP (1.81 mmol/g_{metal}/h) and Ni/HAP catalysts (2.26 mmol/g_{metal}/h), indicating that the catalytic activity of bimetallic CoNi active sites is better than that of monometallic Ni or Co. Moreover, the product distribution of these catalysts is quite different. For the Co/HAP catalyst, it can simultaneously produce ODL and HP with similar selectivity. However, for the Ni/HAP catalyst, except for SA produced by hydrolysis, HP is almost the only product, confirming that Ni has strong C═O and C—C bonds activation ability. On this basis, the incorporation of Ni to Co could greatly promote the hydrodecarboxylation or hydrodecarbonylation reaction (Fig. S1), resulting in the extremely high HP selectivity (98.2%) over the Co_5Ni_5/HAP catalyst. Notably, the catalytic activity and HP selectivity of the Co_5Ni_5/HAP (mix) catalyst prepared by mechanical mixing are similar to those of the monometallic Co/HAP and Ni/HAP catalysts. This indicates that there is a synergistic catalytic effect between Ni and Co rather than a simple superposition. Preliminary results motivate us to further study the potential structure-activity/selectivity relationship for the hydrodeoxygenation of MS to HP.

3.2. Physical structure properties of the CoNi/HAP catalysts

TEM was first performed to explore the growth behavior of Co and Ni species on the HAP support. Fig. 2 shows that the Co/HAP catalyst exhibits uniform dispersed Co metal nanoparticles at approximately 18.4 nm, and the introduction of Ni does not significantly change the particle size (~ 18.0 nm). However, the incorporation of excessive Ni could easily lead to the increase of particle size of nanoparticles (> 21.0 nm over the Co_2Ni_8/HAP catalyst), and even the Ni nanoparticles on the Ni/HAP catalyst are agglomerated. It is highly possible that the Ni nanoparticles with the large surface energy is in an energy unstable state on the surface of HAP support, resulting in the easy sintering during heat treatment [40,41].

Meanwhile, the particle size of the CoNi/HAP catalysts is correlated with the initial reaction rate. Although the particle size increases with the introduction of Ni, the initial reaction rate first increases and then decreases, and the Co_5Ni_5/HAP catalyst exhibits the highest initial

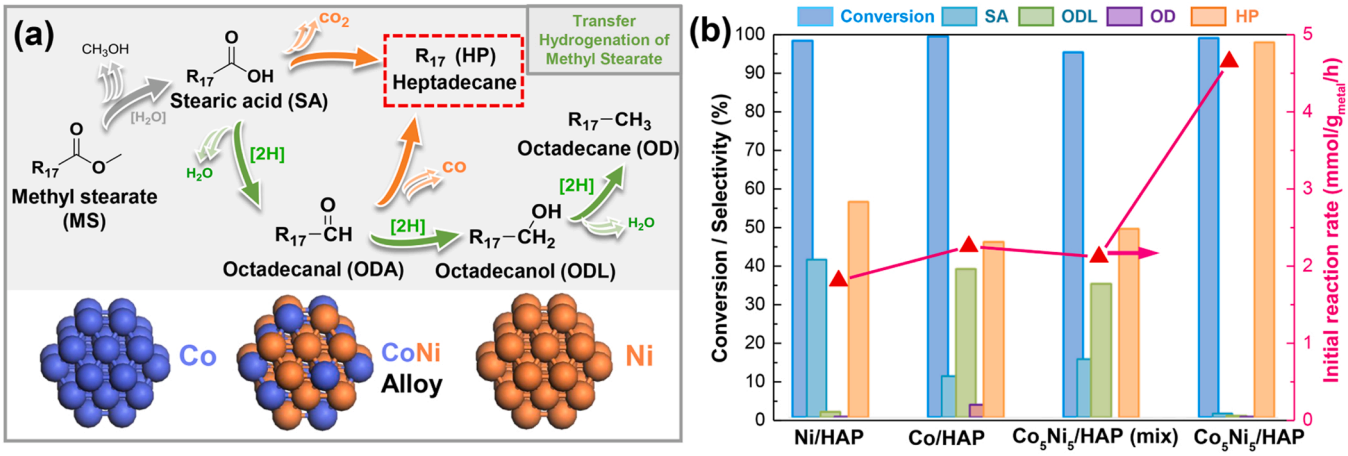

Fig. 1. (a) Schematic diagram of the hydrogenation of methyl ester to different products. (b) Catalytic performance for hydrogenation of methyl ester over Ni/HAP, Co/HAP. Co_5Ni_5/HAP (mix) and Co_5Ni_5/HAP catalysts (reaction conditions: 0.3 g MS, 0.2 g catalyst, 10 mL hexane, 20 mL H_2O, 3 mL methanol, 290 °C and 10 h).

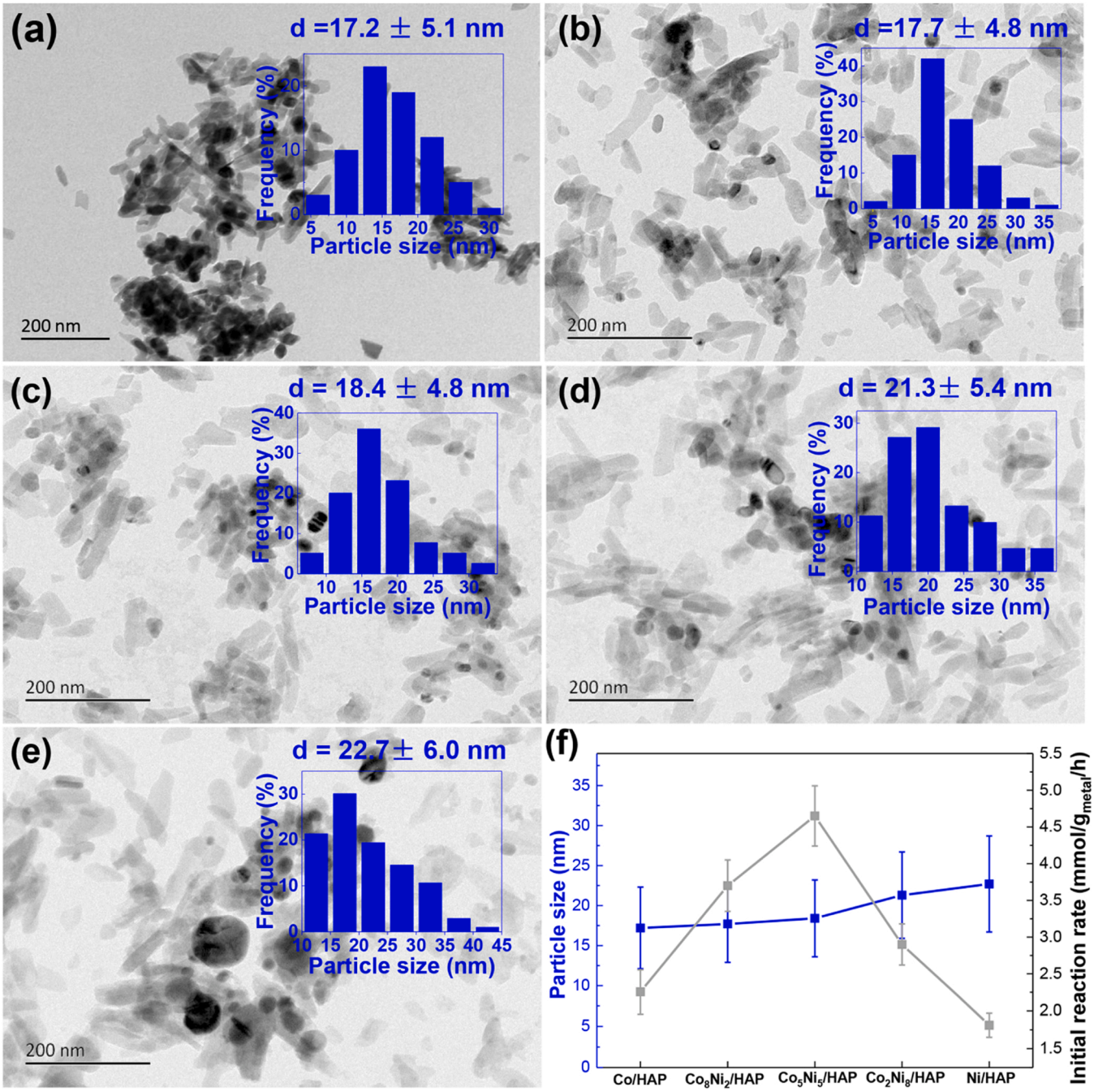

Fig. 2. TEM images and particle size distribution of (a) Co/HAP, (b) Co_8Ni_2/HAP, (c) Co_5Ni_5/HAP, (d) Co_2Ni_8/HAP and (e) Ni/HAP catalysts. (f) Relationship between particle size and initial reaction rate of the CoNi/HAP catalysts.

reaction rate. There is no obvious relationship between the particle size and initial reaction rate, proving that the size effect is not the decisive factor affecting the catalytic activity.

The crystallinity of bimetallic CoNi/HAP catalysts was further confirmed by XRD. Fig. 3a shows that typical diffraction peaks of hexagonal HAP crystal phase are characterized at $2\theta = 26.0°$, 31.8°, 32.4°, 33.0°, 47.5° and 49.0° (JCPDS: 01-082-2956) [42,43]. Meanwhile, the Co/HAP and Ni/HAP catalysts display characteristic diffraction peaks belonging to Co(111) and Ni(111) at 44.2° and 44.7° respectively. There is only one diffraction peak between 44.2° and 44.7° on the bimetallic CoNi/HAP catalysts. It is highly possible that the lattice structure of Co (111) and Ni (111) are distorted, leading to the formation of CoNi alloy nanoparticles [35]. Fig. 3b shows that Co (red) and Ni (violet) are uniformly distributed on the same nanoparticles without obvious segregation in the Co_5Ni_5/HAP catalyst. HRTEM in Fig. 3c also shows that only one kind of lattice spacing (~ 0.208 nm) belonging to Co/Ni (111) could be observed in the Co_5Ni_5/HAP catalyst. Moreover, the element line scanning clearly reveals that both Co and Ni are distributed throughout the nanoparticles (Fig. S2). All these provide strong evidence for the formation of CoNi alloy nanoparticles in the CoNi/HAP catalysts. In addition, it should be noted that pure Co metal has two crystal structures: fcc structure above the isomer transition temperature (~ 420 °C), and hcp structure below this temperature [37]. Generally, nano Co nanoparticles could maintain the high temperature fcc structure at room temperature under the alloying effect of Ni or other metals [34–36, 38,39]. Therefore, it can be concluded that CoNi alloy nanoparticles with fcc structure are formed on the bimetallic CoNi/HAP catalysts.

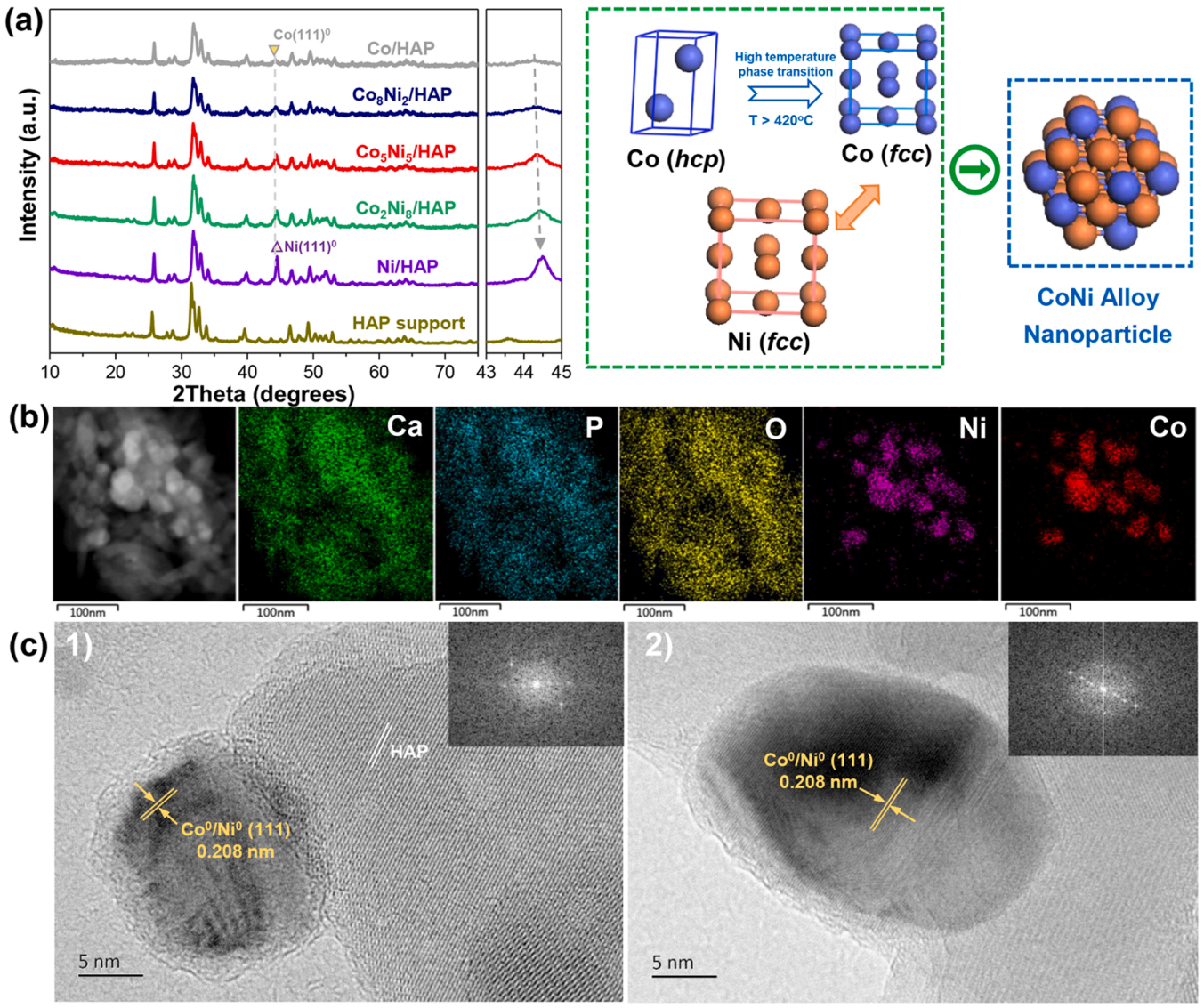

Fig. 3. (a) XRD patterns of the CoNi/HAP catalysts. (b) EDX-mapping and (c) HRTEM images of the Co_5Ni_5/HAP catalyst.

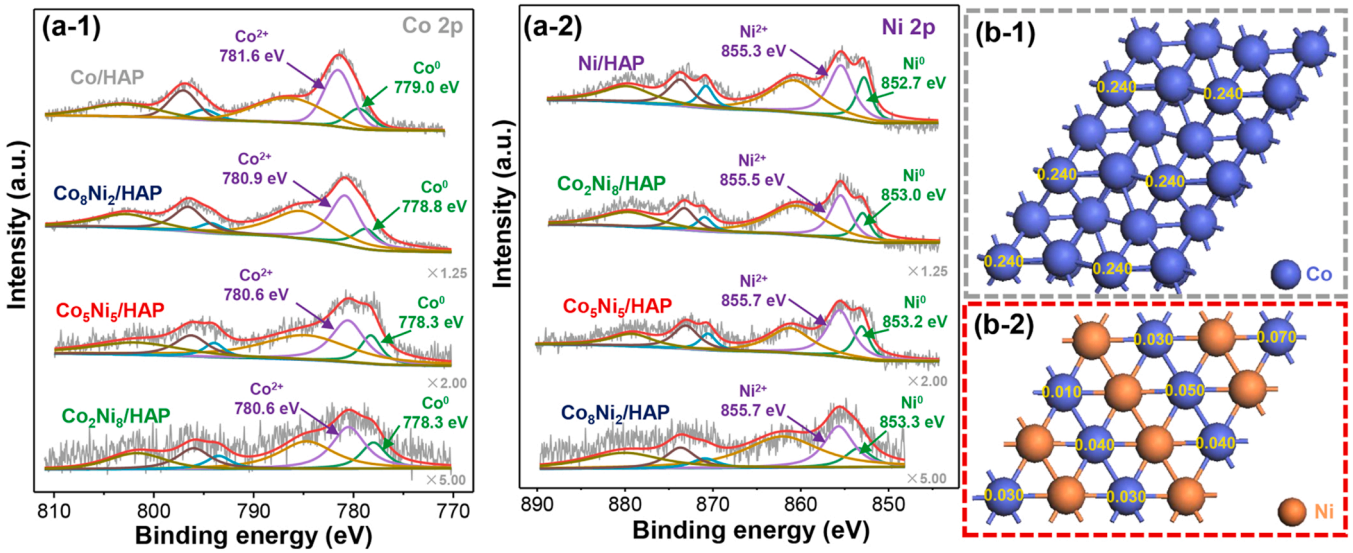

Fig. 4. XPS spectra of (a-1) Co 2p and (a-2) Ni 2p of the CoNi/HAP catalysts. (b) Mulliken charge (|e|) distribution of (b-1) Co (111) and (b-2) CoNi (111) models.

3.3. Chemical structure properties of the CoNi/HAP catalysts

The chemical states of surface Co and Ni elements on the CoNi/HAP catalysts were determined by XPS. Fig. 4a shows that the Co 2p and Ni 2p spectra could be deconvolved into two main peaks, including Co^0 (~ 778.5 eV), Co^{2+} (~ 781.5 eV) and Ni^0 (~ 853.0 eV), Ni^{2+} (~ 855.3 eV), respectively, along with two additional satellites [26]. With the addition of Ni, the binding energies of Co^0 and Co^{2+} in the CoNi/HAP catalysts decrease compared with that of Co/HAP catalyst. In contrast, the binding energies of Ni^0 and Ni^{2+} increase obviously. This indicates that there is an electron transfer from Ni to Co due to the incorporation of Ni to Co. In particular, the Co_5Ni_5/HAP catalyst exhibits the strongest electron coupling effect due to its lowest binding energy of Co and Ni species. In addition, Table S4 shows that the surface content of Co^0 increases significantly after the addition of Ni, suggesting that the presence of Ni could promote the reduction of CoNi alloy nanoparticles. The surface electronic properties were further investigated by DFT calculation to better understand the electronic modification of CoNi nanoparticles (Figs. S3 and 4b). Fig. 4b shows that the Co atoms on the surface of Co (111) model have a small amount of positive charge (0.240 |e|). Following the addition of Ni, the positive charge of Co on the surface of CoNi(111) model decreases to electric neutrality, which is consistent with the conclusion of electron transfer from Ni to Co in the bimetallic CoNi/HAP catalysts characterized by XPS. It has been demonstrated that the enrichment of electrons on the metal surface tends to enhance the adsorption of oxygen-containing substrate and promote its activation [44,45]. Therefore, the strong electronic coupling effect of the bimetallic CoNi/HAP catalysts may be closely related to the improvement of catalytic activity of MS hydrodeoxygenation, which will be confirmed by our following detailed DFT calculation.

Subsequently, H_2-TPR, CO-TPD and CO_2-TPD were employed to further elucidate the surface chemical properties of the CoNi/HAP catalysts. Fig. 5a shows that the Co/HAP catalyst exhibits two H_2 reduction peaks, corresponding to the reduction of Co_3O_4 to CoO (~ 280 °C) and CoO to Co (~ 380 °C) [46–48]. For the monometallic Ni/HAP catalyst, only one H_2 reduction peak appeared near 376 °C, corresponding to the reduction of NiO to metallic Ni. Obviously, the introduction of Ni decreases the reduction temperature of Co species, indicating that the CoNi alloy nanoparticles could be easily reduced compared to the Co nanoparticles [46]. Combined with the previous characterization results, it is highly possible that the structural reconstruction (the formation of new fcc structure) during the formation of CoNi alloy nanoparticles leads to the change of reduction properties. Then, the surface active sites for adsorption of CO and CO_2 were investigated by CO-TPD and CO_2-TPD. Fig. 5b shows that the introduction of Ni increases the desorption temperature of CO, suggesting that the bimetallic CoNi/HAP catalysts exhibit strong adsorption ability for CO. Fig. 5c shows HAP support exhibits a strong CO_2 adsorption peak at ~200 °C, indicating that it contains many medium strength alkaline sites. It is widely accepted that alkaline sites of Ca in HAP could promote the forward reaction to generate hydrogen via adsorbing CO_2 during methanol and water reforming process [$CH_3OH(g)+H_2O(g) \rightleftharpoons CO_2(g)+3\,H_2(g)$] [49,50].

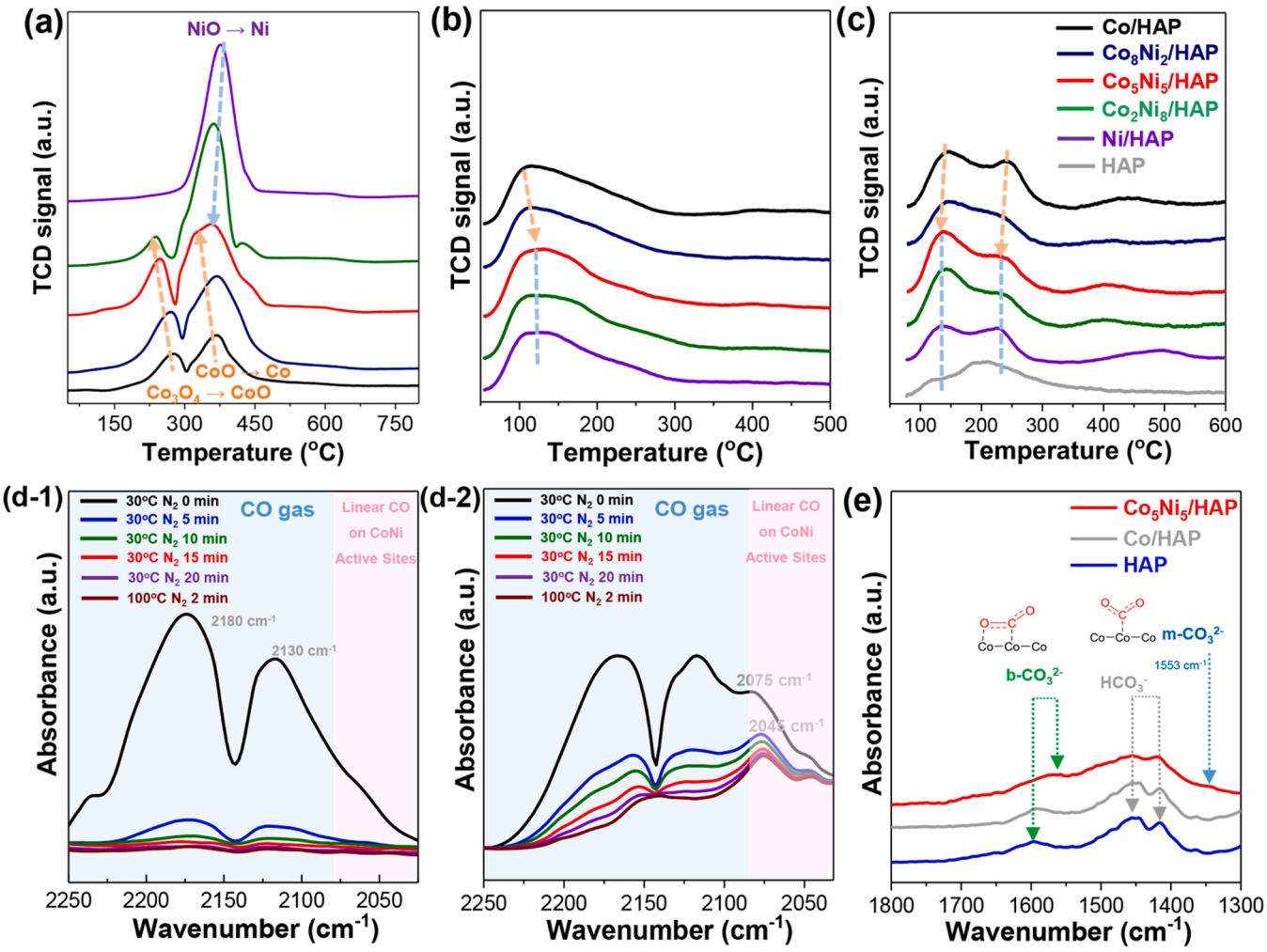

Fig. 5. (a) H_2-TPR, (b) CO-TPD and (c) CO_2-TPD profiles of the CoNi/HAP catalysts. In situ FT-IR spectra of (d) CO and (e) CO_2 of the Co/HAP and Co_5Ni_5/HAP catalysts.

Therefore, the Co_5Ni_5/HAP catalyst with basic HAP support displays superior catalytic performance for catalytic transfer hydrogenation of MS than the Co_5Ni_5/AC and Co_5Ni_5/SiO_2 catalyst (Table S5). Meanwhile, the desorption temperature of CO_2 on the bimetallic CoNi/HAP catalysts is lower than that on the Co/HAP catalyst, indicating that the introduction of Ni weakens the adsorption ability of CO_2. When the mass ratio of Co/Ni is 1:1, the desorption properties of CO and CO_2 do not change with the further introduction of Ni. It should be noted that the adsorption ability for CO and CO_2 over the bimetallic CoNi/HAP catalyst could reflect the reaction pathway of the hydrodeoxygenation of MS to HP (decarbonylation (-CO) or decarboxylation (-COO)) [51]. According to the conclusion of CO-TPD and CO_2-TPD, the addition of Ni promotes the formation of HP by decarbonylation rather than decarboxylation.

To further confirm this point, in situ CO and CO_2 FT-IR spectra were employed to investigate the adsorption behavior of the bimetallic CoNi/HAP catalysts. Fig. 5d shows that both the Co/HAP and Co_5Ni_5/HAP catalysts displays the adsorption bands of gas phase CO in the initial desorption stage, with peak positioned at 2100–2250 cm^{-1} [52]. With the prolongation of N_2 purge time, the adsorption band of gas phase CO on the Co/HAP catalyst weakens and disappears, indicating a weak interaction between CO and Co active sites (Fig. 5d-1). In contrast, two narrow, quasi-symmetrical bands at 2075 and 2045 cm^{-1} are observed on the Co_5Ni_5/HAP catalyst, which could be rationally ascribed as linearly absorbed CO on the metal active sites (Fig. 5d-2) [52]. This suggests that the introduction of Ni enhances the adsorption ability of the Co_5Ni_5/HAP catalyst for CO. Meanwhile, in situ CO_2 FT-IR spectra in Fig. 5e show that the CO_2 adsorption bands of the Co/HAP catalyst are similar to that of the HAP support, including the bidentate carbonate (b-CO_3^{2-}, at 1596 cm^{-1}) and bicarbonate (HCO^{3-}, at 1448 and 1413 cm^{-1}) [53–55]. For the Co_5Ni_5/HAP catalyst, the intensity of overall CO_2 absorption bands is weaker than that of the Co/HAP catalyst, and the adsorption band of monodentate carbonate (m-CO_3^{2-}, at 1550 cm^{-1}) with weak adsorption ability is observed, revealing the poor CO_2 adsorption ability [53]. On these foundations, it can be concluded that the introduction of Ni enhances the adsorption of CO and weakens the adsorption of CO_2, confirming that the formation of HP over the Co_5Ni_5/HAP catalyst is mainly through the decarbonylation reaction rather than decarboxylation reaction.

3.4. Structure-dependent kinetics on the CoNi/HAP catalysts

Since the presence of Ni promoted the catalytic performance of the catalytic transfer hydrogenation of MS to HP, the effect of Ni on the kinetic behavior of the bimetallic CoNi/HAP catalysts was synergistically investigated. Figs. S4a and 6a show that the MS conversion of the Co/HAP and Co_5Ni_5/HAP catalysts increases rapidly with the increase of reaction temperature, and a higher MS conversion could be obtained at low temperature (< 290 °C) over the Co_5Ni_5/HAP catalyst, suggesting that the Co_5Ni_5/HAP catalyst exhibits higher catalytic activity than the Co/HAP catalyst. Subsequently, the product selectivity of the two catalysts under the influence of reaction temperature is further analyzed. It should be noted that SA is the product of MS hydrolysis, even without the presence of catalyst, MS could still quickly generate a large amount of SA (Table S2). As a result, the catalytic performance of catalytic

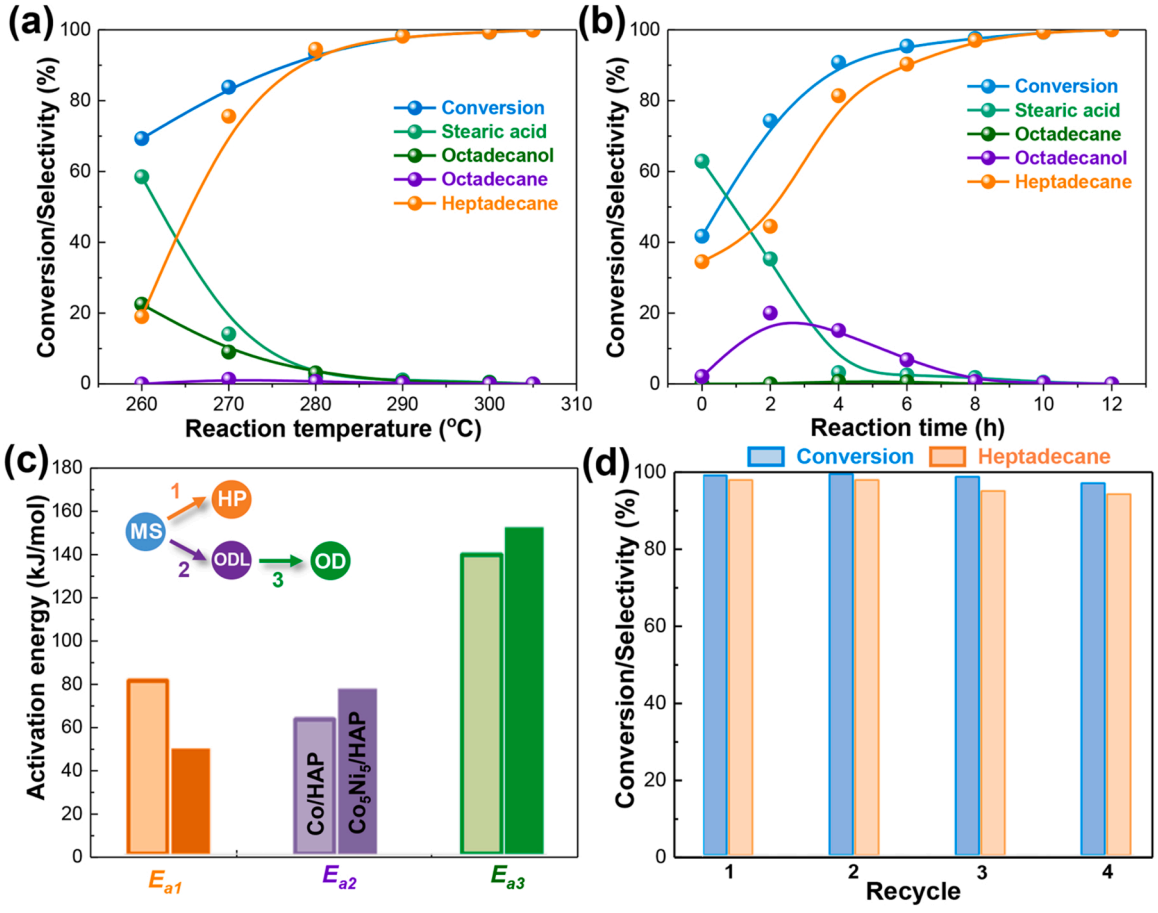

Fig. 6. Catalytic performance for hydrogenation of methyl ester over the Co_5Ni_5/HAP catalyst as a function of (a) reaction temperature (reaction conditions: 0.3 g MS; 0.2 g cat.; 3 mL methanol; 10 mL hexane; 20 mL water; 8 h) and (b) reaction time (reaction conditions: 0.3 g MS; 0.2 g cat.; 3 mL methanol; 10 mL hexane; 20 mL water; 290 °C). (c) Apparent activation energies based on 270–310 °C (reaction conditions: 0.3 g MS; 0.2 g cat.; 3 mL methanol; 10 mL hexane; 20 mL water). (d) Catalyst stability of the Co_5Ni_5/HAP catalyst (reaction conditions: 0.3 g MS; 0.2 g cat.; 3 mL methanol; 10 mL hexane; 20 mL water; 290 °C; 8 h).

transfer hydrogenation using SA as the reaction substrate is almost the same as that using MS as the reaction substrate. In other words, SA tends to be the equilibrium product of MS without hydrogenation [7,12]. Interestingly, the product (except SA) selectivity of the two catalysts displays a significant difference with the increase of reaction temperature. For the Co/HAP catalyst, ODL is the main product, and the ODL selectivity increases first and then decreases with the increase of reaction temperature. For the Co_5Ni_5/HAP catalyst, both ODL and HP are the main products of MS transfer hydrogenation at low temperature, and the HP selectivity increases rapidly with the increase of reaction temperature. These indicate that ODL and HP are parallel products of MS transfer hydrogenation, and the HP selectivity is significantly improved by the introduction of Ni.

To further confirm these points, conversion/selectivity–time profiles on these two catalysts were obtained. Undoubtedly, with the extension of reaction time, the conversion of MS on the Co/HAP and Co_5Ni_5/HAP catalysts increases rapidly, and almost completely conversion of MS could be achieved after the reaction time $\geq$ 8 h (Figs. S4b and 6b). Moreover, the product distributions of ODL and HP on the Co/HAP and Co_5Ni_5/HAP catalysts show similar trends with the increase of reaction time: ODL increases first and then decreases, while HP increases continuously. In the initial reaction stage (0–4 h), both ODL and HP are the main products on the two catalysts, confirming that ODL and HP are the parallel products of MS catalytic transfer hydrogenation. With the prolong of reaction time (4–8 h), ODL is the main product on the Co/HAP catalyst, and HP is the main product on the Co_5Ni_5/HAP catalyst, revealing that the addition of Ni could significantly promote the formation of HP instead of ODL in the catalytic transfer hydrogenation of MS. When the reaction time is further prolonged ($>$ 8 h), the ODL selectivity on the Co/HAP catalyst decreases and the selectivity of HP and OD increases, indicating that ODL could be further hydrogenated to HP and OD under the condition of deep hydrogenation. Supplementary evaluation experiments using ODL as substrate (Table S2) show that MS, SA and ODA could be easily obtained by the reverse reaction of ODL on the Co/HAP catalyst, and the conversion of OD on the Co/HAP catalyst is only 35%, accompanied by 20.5% HP selectivity, indicating that the catalytic activity for further hydrodecarboxylation of ODL is limited. In contrast, HP is almost the only hydrogenation product on the Co_5Ni_5/HAP catalyst, suggesting that the reaction pathway for the catalytic transfer hydrogenation of MS has been significantly tuned on the bimetallic CoNi active sites.

The apparent reaction kinetics was further employed to intuitively reveal the change of reaction pathway caused by the introduction of Ni. The reaction network involving the hydrodecarbonylation of MS to HP and MS sequential hydrogenation to ODL and OD is proposed, and the estimated apparent activation energies for MS→HP, MS→ODL and ODL→HP on the two catalysts are listed in Fig. 6c. It is found that the activation energy of MS→ODL on the Co/HAP catalyst (63.2 kJ/mol) is significantly lower than that of MS→HP (81.0 kJ/mol), while the opposite trend is observed on the Co_5Ni_5/HAP catalyst. This further confirms that ODL and HP are the main products on the Co/HAP and Co_5Ni_5/HAP catalysts, respectively. Moreover, the Co_5Ni_5/HAP catalyst exhibits much lower activation energy of MS→HP (49.5 kJ/mol) than the Co/HAP catalyst (81.0 kJ/mol), indicating that the introduction of Ni enhances the hydrodecarbonylation ability of MS. In addition, both the Co/HAP and Co_5Ni_5/HAP catalysts display high activation energy of ODL→HP ($>$ 100 kJ/mol), revealing that further hydrodecarboxylation of ODL to OD is difficult.

Then, the catalyst stability of the Co/HAP and Co_5Ni_5/HAP catalysts in the catalytic transfer hydrogenation of MS was investigated. Fig. S4c shows that the conversion and ODL selectivity on the Co/HAP catalyst decrease with the increase of the recycle number. After characterization of the used Co/HAP catalyst, the valence of Co does not change significantly (Fig. S5 and Table S6), while the loading of Co metal decreases from previous 9.6–8.5%, suggesting that the loss of Co leads to the decrease of catalytic performance. In sharp contrast, the MS conversion and HP selectivity on the Co_5Ni_5/HAP catalyst remain almost unchanged with the increase of the recycle number (Fig. 6d). Fig. S5 shows that the crystallinity, the metal loading of Co and Ni, and the valence of Co and Ni on the surface of the used Co_5Ni_5/HAP catalyst are almost unchanged. It has been demonstrated that HAP support with good thermal stability and low water solubility displays unique advantages in immobilizing Co based metals for the hydrogenation of fatty acids [12,56,57]. Notably, Fig. S5 shows that the particle size of the used Co_5Ni_5/HAP catalyst increases from previous 18.4–24.9 nm. Previous discussions (in Fig. 2) have shown that particle size (at least about 20 nm) is not an important factor affecting the performance of MS transfer hydrogenation. In addition, even if the particles are agglomerated, the CoNi particles with almost no metal leaching still exist stably in the form of alloy. This further confirmed that the CoNi alloy particles with strong electronic coupling effect are the key to the transfer hydrogenation of methyl stearate to heptadecane. Consequently, the Co_5Ni_5/HAP catalyst with CoNi alloy nanoparticles exhibits superior catalyst stability.

Given our interest in the catalytic transfer hydrogenation of MS to HP, we compared the catalytic performance of the optimal Co_5Ni_5/HAP catalyst with previously reported catalysts. Table S7 shows that noble metal catalysts exhibits high catalytic activity, and ~90% HP yield could be obtained on the PdNi/HZSM-5 and Ni-Pt-ALD catalysts [58,59]. However, among the numerous non noble metal catalysts, only bimetallic CuNi catalysts can improve the HP yield to more than 90% [10,11]. Herein, the Co_5Ni_5/HAP catalyst prepared by us achieves a record high HP yield ($>$ 97%) in the catalytic transfer hydrogenation system. Furthermore, for the first time, the efficient hydrodecarbonylation of MS to HP could be realized over the Co-based catalyst due to the addition of Ni.

3.5. *Hydrodecarbonylation mechanism on the Co_5Ni_5/HAP catalysts*

DFT calculation was severed as a powerful tool to explore the reaction mechanism of the hydrogenation of MS to HP at the molecular level. Since methyl stearate could be easily hydrolyzed to stearic acid at high temperature, low carbon carboxylic acid with the same functional groups (-COOH) as stearic acid should be selected as the model compound to improve the efficiency of theoretical calculation. By testing the electronic structure and the adsorption energies of carboxylic acids with different carbon chain lengths over the CoNi (111) surface (Fig. S6), propionic acid (PA) was selected as the simplified model compound in the following calculation process [60,61]. Fig. 7a shows that the CoNi (111) model exhibits much higher adsorption energy of PA (−1.2 eV) than the Co(111) model (−0.7 eV). Combined with the results of XPS and Mulliken charge, it can be inferred that the introduction of Ni strengthens the electron coupling effect and promotes the adsorption of reaction substrate, resulting in the high catalytic activity. The detailed elementary reaction steps of MS to HP over the Co(111) and CoNi(111) models were proposed. For the hydrodecarboxylation of PA to ethane (Fig. 7b), the activation energies of the rate-determine step in this reaction pathway (RCH_2COO^*→RCH_2 *+CO_2 *) over the Co(111) and CoNi(111) models are as high as 3.2 and 3.4 eV, respectively, indicating that decarboxylation reaction is difficult to occur on the Co/HAP and Co_5Ni_5/HAP catalysts. Subsequently, the reaction pathway of PA hydrogenation to n-propanol is shown in Fig. 7c. The introduction of Ni to Co changes the rate-determine step of PA hydrogenation to n-propanol from RCH_2COOH^* →RCH_2O^* +H_2O^* on the Co(111) model (1.5 eV) to RCH_2CHOH^* +H* →$RCH_2CH_2OH^*$ on the CoNi(111) model (1.8 eV). Obviously, the presence of Ni enhances the hydrogenation of PA to remove OH over the electron enriched Co active site, while the hydrogenation ability of oxygen-containing intermediates (RCH_2CHOH) is inhibited during the formation of n-propanol. Meanwhile, compared with the CoNi(111) model, the Co (111) model displays a lower activation energy of the rate-determine step. This means that ODL tends to be formed on the Co/HAP catalyst instead of the Co_5Ni_5/HAP catalyst. Notably, if the RCH_2CO^* intermediate (obtained in the process of PA to

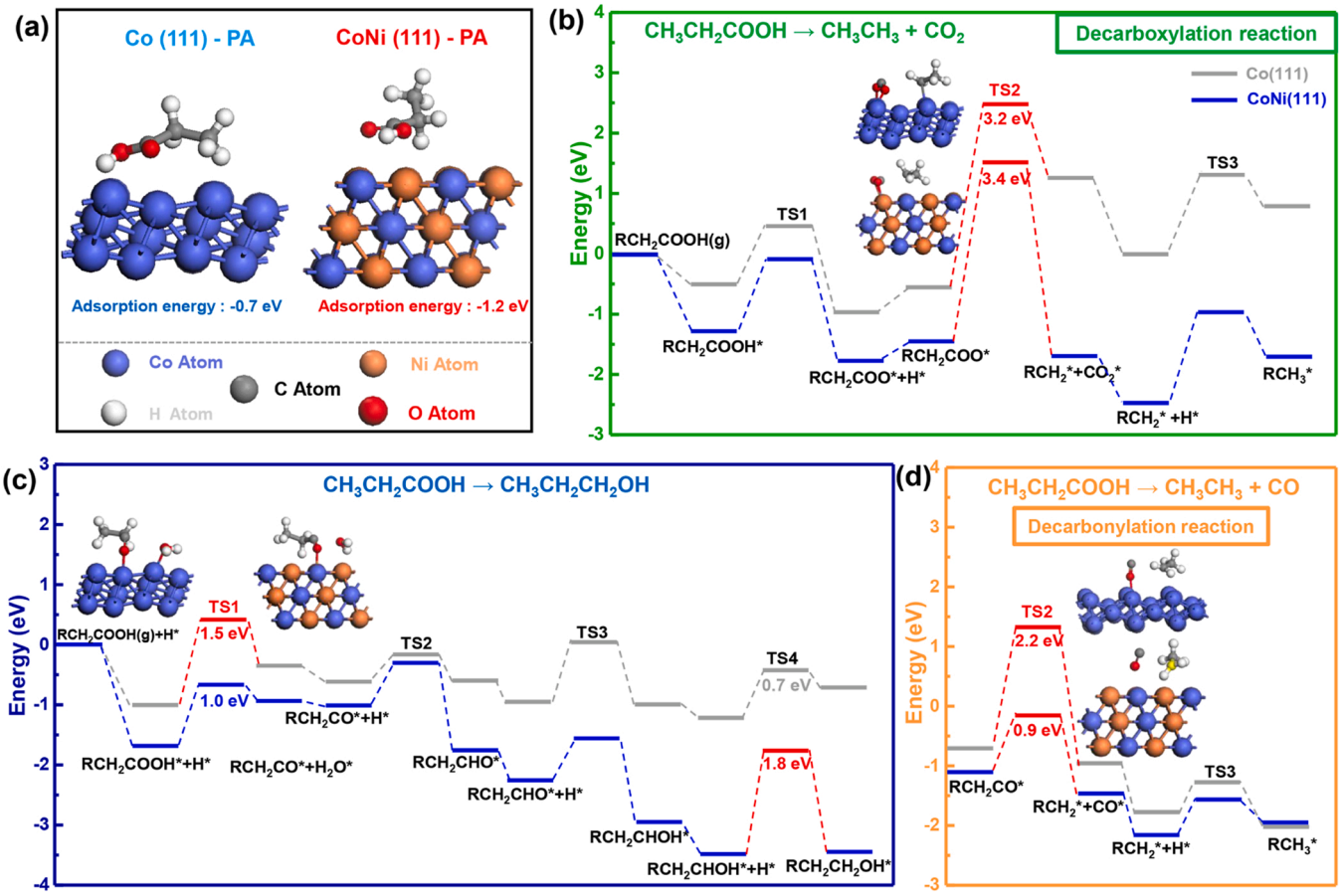

Fig. 7. (a) Adsorption energy of propionic acid (PA) on the Co (111) and CoNi (111) models. Energy profiles for (b) propionic acid hydrogenation to propanol, (c) propionic acid hydro-decarboxylation to ethane and (d) propionic acid hydrodecarbonylation to ethane.

propionaldehyde) is directly hydrogenated and decarbonylated to ethane, the activation energy of $RCH_2CO^* \rightarrow RCH_2{}^* + CO^*$ on the CoNi (111) model is only 0.9 eV, which is far less than that on the Co(111) model (2.2 eV). This indicates that the Ni active site promotes the cleavage of C—C bond cleavage of RCH_2CO intermediate, inducing the formation of ethane rather than n-propanol. Therefore, the CoNi alloy nanoparticles on the Co_5Ni_5/HAP catalyst mainly enhance the adsorption of substrate and promote the hydrodecarbonylation process, resulting in the improvement of the catalytic performance for catalytic transfer hydrogenation of MS to HP.

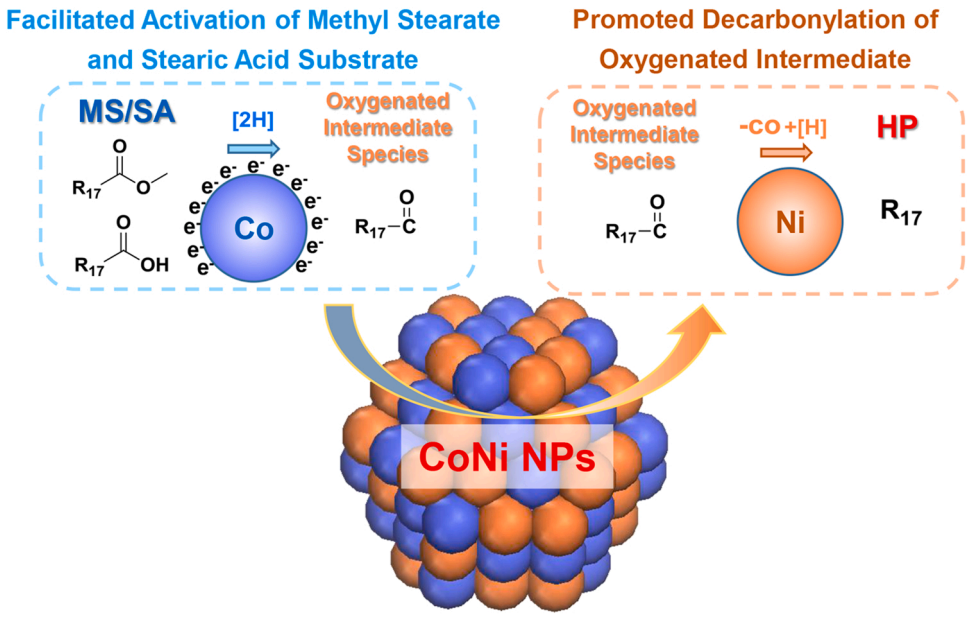

Fig. 8. Plausible reaction mechanism of stearic acid substrate to heptadecane over the bimetallic CoNi/HAP catalysts.

Finally, the reaction mechanism of the catalytic transfer hydrogenation of MS to HP on the bimetallic CoNi/HAP catalysts is summarized in Fig. 8. The introduction of Ni strengthens the electron coupling effect of the CoNi alloy nanoparticles, and promotes the adsorption of MS/SA, resulting in the improvement of catalytic activity. Commonly, there are usually two reaction pathways for MS hydrogenation: one is the hydrogenation of MS to ODL and then to HP; the other is the direct hydrodecarbonylation of MS to HP. Further analysis of the detailed elementary reaction steps shows that the introduction of Ni changes the reaction pathway of MS hydrogenation from MS→ODL over the Co/HAP catalyst to MS→HP over the Co_5Ni_5/HAP catalyst. Moreover, it is found that the formation of HP over the bimetallic CoNi/HAP catalysts is mainly through hydrodecarbonylation (-CO) rather than hydrodecarboxylation (-COO). During the hydrogenation process, Co metal active site promotes the formation of oxygen-containing intermediates before ODL, and the as-formed C—C bond of the oxygenated intermediate (RCH_2CO) tends to be activated on the Ni active site of CoNi alloy nanoparticles, leading to the high HP selectivity. On these foundations, the Co_5Ni_5/HAP catalyst exhibits high catalytic activity and HP selectivity for the catalytic transfer hydrogenation of MS.

4. Conclusions

In conclusion, the bimetallic CoNi/HAP catalysts were prepared for the catalytic transfer hydrogenation of methyl stearate to heptadecane. Under strong reduction conditions of the incipient wetness impregnation method, CoNi alloy nanoparticles with fcc structure could be formed on the bimetallic CoNi/HAP catalysts. Surface characterizations show that the addition of Ni to Co induces the strong electron coupling effect and enhance the adsorption of methyl stearate or stearic acid, leading to the improvement of catalytic activity. Meanwhile, the reaction pathway for the catalytic transfer hydrogenation of methyl stearate has been significantly tuned on the bimetallic CoNi active sites. The hydrogenation of methyl stearate to heptadecane instead of octadecanol becomes the main reaction pathway over the bimetallic CoNi/HAP catalysts. Moreover, the introduction of Ni promotes the C—C bond cleavage of RCH_2CO intermediate, resulting in the high heptadecane selectivity. Consequently, the Co_5Ni_5/HAP catalyst displays 99% conversion and 98% selectivity of heptadecane under the optimized conditions (290 °C and 8 h). These results obtained in this work may provide some insights into rational design for high effective catalyst for the catalytic transfer hydrogenation of fatty acids/esters.

CRediT authorship contribution statement

Hao Yan: Conceptualization, Methodology, Investigation, Writing – original draft. **Shuang Yao:** Methodology**,** Formal analysis, Investigation. **Tong Zhang:** Conceptualization. **Delong Li:** Investigation**. Xiaoyu Tang:** Investigation**. Mengxin Chen:** Supervision, Funding acquisition. **Yixuan Zhou:** Project administration Validation. **Mingrui Zhang:** Writing – review & editing**. Yibin Liu:** Writing – review & editing**. Xin Zhou:** Investigation**. Xiang Feng:** Writing – review & editing**. Xiaobo Chen:** Formal analysis**. Chaohe Yang:** Supervision, Funding acquisition, Validation.

Declaration of Competing Interest

All the authors declare no conflict of interest.

Acknowledgments

Our work was supported by the Independent Innovation Research Projects (20CX06072A, 20CX06095A and 20CX06096A), Natural Science Foundation of Shandong Province (ZR2021QB076 and ZR2020YQ17), China Postdoctoral international exchange program (2020072), Qingdao Postdoctoral Funded Project (qdyy20200069 and qdyy20200073) and National Natural Science Foundation of China (22108305, 21978325 and 22108307).

Appendix A. Supplementary material

Supplementary characterizations with HRTEM, BET, XRD, H2-TPR, H2-TPD and XPS; calculation process of reaction kinetics; supplementary comparative experimental results; comparison of catalytic performance with other reported catalysts.

Supplementary data associated with this article can be found in the online version at doi:10.1016/j.apcatb.2022.121138.

References

[1] H. Yan, S. Yao, J. Wang, S. Zhao, Y. Sun, M. Liu, X. Zhou, G. Zhang, X. Jin, X. Feng, Y. Liu, X. Chen, D. Chen, C. Yang, Engineering Pt-Mn2O3 interface to boost selective oxidation of ethylene glycol to glycolic acid, Appl. Catal. B 284 (2021), 119803.
[2] B. Boekaerts, B.F. Sels, Catalytic advancements in carboxylic acid ketonization and its perspectives on biomass valorization, Appl. Catal. B 283 (2021), 119607.
[3] K. Su, Y. Wang, C. Zhang, Z. Gao, J. Han, F. Wang, Tuning the Pt species on Nb2O5 by support-induced modification in the photocatalytic transfer hydrogenation of phenylacetylene, Appl. Catal. B 298 (2021), 120554.
[4] D. Jiraroj, O. Jirarattanapochai, W. Anutrasakda, J.S.M. Samec, D.N. Tungasmita, Selective decarboxylation of biobased fatty acids using a Ni-FSM-16 catalyst, Appl. Catal. B 291 (2021), 120050.
[5] L. Wang, X. Niu, J. Chen, SiO2 supported Ni-In intermetallic compounds: efficient for selective hydrogenation of fatty acid methyl esters to fatty alcohols, Appl. Catal. B 278 (2020), 119293.
[6] Y. Zhou, L. Liu, G. Li, C. Hu, Insights into the influence of ZrO2 crystal structures on methyl laurate hydrogenation over Co/ZrO2 catalysts, ACS Catal. 11 (2021) 7099–7113.
[7] Z. Zhang, M. Jing, H. Chen, F. Okejiri, J. Liu, Y. Leng, H. Liu, W. Song, Z. Hou, X. Lu, J. Fu, J. Liu, Transfer hydrogenation of fatty acids on Cu/ZrO2: demystifying the role of carrier structure and metal–support interface, ACS Catal. 10 (2020) 9098–9108.
[8] X. Zhou, H. Yan, X. Feng, H. Zhao, Y. Liu, X. Chen, D. Chen, C. Yang, Producing glyceric acid from glycerol via integrating vacuum dividing wall columns: conceptual process design and techno-economic-environmental analysis, Green Chem. 23 (2021) 3664–3676.
[9] H. Yan, Q. Shen, Y. Sun, S. Zhao, R. Lu, M. Gong, Y. Liu, X. Zhou, X. Jin, X. Feng, X. Chen, D. Chen, C. Yang, Tailoring facets of α-Mn2O3 microcrystalline catalysts for enhanced selective oxidation of glycerol to glycolic acid, ACS Catal. 11 (2021) 6371–6383.
[10] J. Wang, L. Xu, R. Nie, X. Lyu, X. Lu, Bifunctional CuNi/CoOx catalyst for mild-temperature in situ hydrodeoxygenation of fatty acids to alkanes using isopropanol as hydrogen source, Fuel 265 (2020), 116913.
[11] Z. Zhang, H. Chen, C. Wang, K. Chen, X. Lu, P. Ouyang, J. Fu, Efficient and stable Cu-Ni/ZrO2 catalysts for in situ hydrogenation and deoxygenation of oleic acid into heptadecane using methanol as a hydrogen donor, Fuel 230 (2018) 211–217.
[12] S. Yao, T. Zhang, X. Tang, D. Li, W. Zhang, D. Lin, R. Li, H. Yan, Y. Liu, X. Feng, X. Chen, X. Zhou, C. Yang, Octadecanol production from methyl stearate by catalytic transfer hydrogenation over synergistic Co/HAP catalysts, Energy Fuel 35 (2021) 9970–9982.
[13] J. Wang, G. Zhang, M. Liu, Q. Xia, X. Yu, W. Zhang, J. Shen, C. Yang, X. Jin, Lattice distorted MnCo oxide materials as efficient catalysts for transfer hydrogenation of levulinic acid using formic acid as H-donor, Chem. Eng. Sci. 222 (2020), 115721.
[14] J. Wang, R. Nie, L. Xu, X. Lyu, X. Lu, Catalytic transfer hydrogenation of oleic acid to octadecanol over magnetic recoverable cobalt catalysts, Green Chem. 21 (2019) 314–320.
[15] I. Hachemi, N. Kumar, P. Mäki-Arvela, J. Roine, M. Peurla, J. Hemming, J. Salonen, D.Y. Murzin, Sulfur-free Ni catalyst for production of green diesel by hydrodeoxygenation, J. Catal. 347 (2017) 205–221.
[16] L. Di, S. Yao, S. Song, G. Wu, W. Dai, N. Guan, L. Li, Robust ruthenium catalysts for the selective conversion of stearic acid to diesel-range alkanes, Appl. Catal. B 201 (2017) 137–149.
[17] V.O. Rodina, D.Y. Ermakov, A.A. Saraev, S.I. Reshetnikov, V.A. Yakovlev, Influence of reaction conditions and kinetic analysis of the selective hydrogenation of oleic acid toward fatty alcohols on Ru-Sn-B/Al2O3 in the flow reactor, Appl. Catal. B 209 (2017) 611–620.
[18] Z. Zhang, Z. Chen, H. Chen, X. Gou, K. Chen, X. Lu, P. Ouyang, J. Fu, Catalytic decarbonylation of stearic acid to hydrocarbons over activated carbon-supported nicke, Sustain. Energy Fuels 2 (2018) 1837–1843.
[19] C. Miao, O. Marin-Flores, T. Dong, D. Gao, Y. Wang, M. Garcia-Pérez, S. Chen, Hydrothermal catalytic deoxygenation of fatty acid and bio-oil with in situ H2. ACS Sustain. Chem. Eng. 6 (2018) 4521–4530.
[20] Z. Zhang, Q. Yang, H. Chen, K. Chen, X. Lu, P. Ouyang, J. Fu, J.G. Chen, U.N.U. S. Brookhaven National Lab, B.N.L. Zhejiang Univ H.C., T.U.C. Nanjing, In situ hydrogenation and decarboxylation of oleic acid into heptadecane over a Cu–Ni alloy catalyst using methanol as a hydrogen carrier, Green Chem. 20 (2018) 197–205.

[21] V.K. Soni, P.R. Sharma, G. Choudhary, S. Pandey, R.K. Sharma, Ni/Co-natural clay as green catalysts for microalgae oil to diesel-grade hydrocarbons conversion, ACS Sustain. Chem. Eng. 5 (2017) 5351–5359.
[22] A. Ali, B. Li, Y. Lu, C. Zhao, Highly selective and low-temperature hydrothermal conversion of natural oils to fatty alcohols, Green Chem. 21 (2019) 3059–3064.
[23] D.R. Vardon, B.K. Sharma, H. Jaramillo, D. Kim, J.K. Choe, P.N. Ciesielski, T. J. Strathmann, Hydrothermal catalytic processing of saturated and unsaturated fatty acids to hydrocarbons with glycerol for in situ hydrogen production, Green Chem. 16 (2014) 1507–1520.
[24] K.W. Cheah, M.J. Taylor, A. Osatiashtiani, S.K. Beaumont, D.J. Nowakowski, S. Yusup, A.V. Bridgwater, G. Kyriakou, Monometallic and bimetallic catalysts based on Pd, Cu and Ni for hydrogen transfer deoxygenation of a prototypical fatty acid to diesel range hydrocarbons, Catal. Today 355 (2020) 882–892.
[25] X. Gou, F. Okejiri, Z. Zhang, M. Liu, J. Liu, H. Chen, K. Chen, X. Lu, P. Ouyang, J. Fu, Tannin-derived bimetallic CuCo/C catalysts for an efficient in-situ hydrogenation of lauric acid in methanol-water media, Fuel Process. Technol. 205 (2020), 106426.
[26] H. Yan, S. Yao, W. Liang, S. Zhao, X. Jin, X. Feng, Y. Liu, X. Chen, C. Yang, Ni–Co oxide catalysts with lattice distortions for enhanced oxidation of glycerol to glyceric acid, J. Catal. 381 (2020) 248–260.
[27] X. Shi, S.L. Bernasek, A. Selloni, Electronic structure, and defects of Ni substituted spinel cobalt oxide: a DFT+U study, J. Phys. Chem. C 120 (2016) 14892–14898.
[28] J. Lu, S. Behtash, A. Heyden, Theoretical investigation of the reaction mechanism of the decarboxylation and decarbonylation of propanoic acid on Pd(111) model surfaces, J. Phys. Chem. C 116 (2012) 14328–14341.
[29] Z. Han, Z. Yang, M. Han, Comprehensive investigation of methane conversion over Ni(111) surface under a consistent DFT framework: implications for anti-coking of SOFC anodes, Appl. Surf. Sci. 480 (2019) 243–255.
[30] H. Yan, X. Feng, Y. Liu, C. Yang, H. Shan, Catalytic cracking of acetic acid and its ketene intermediate over HZSM-5 catalyst: a density functional theory study, Mol. Catal. 437 (2017) 11–17.
[31] F. Wang, W. Xie, L. Yang, D. Xie, S. Lin, Revealing the importance of kinetics in N-coordinated dual-metal sites catalyzed oxygen reduction reaction, J. Catal. 396 (2021) 215–223.
[32] M. Qu, Y. Jiang, M. Yang, S. Liu, Q. Guo, W. Shen, M. Li, R. He, Regulating electron density of NiFe-P nanosheets electrocatalysts by a trifle of Ru for high-efficient overall water splitting, Appl. Catal. B Environ. 263 (2020), 118324.
[33] H. Zha, X. Dong, Y. Yu, M. Zhang, Hydrogen-assisted versus hydroxyl-assisted CO dissociation over Co-doped Cu(111): A DFT study, Surf. Sci. 669 (2018) 114–120.
[34] M. Qu, Y. Jiang, M. Yang, S. Liu, Q. Guo, W. Shen, M. Li, R. He, Regulating electron density of NiFe-P nanosheets electrocatalysts by a trifle of Ru for high-efficient overall water splitting, Appl. Catal. B 263 (2020), 118324.
[35] U. Kurtan, H. Aydın, B. Büyük, U. Şahintürk, M.A. Almessiere, A. Baykal, Freestanding electrospun carbon nanofibers uniformly decorated with bimetallic alloy nanoparticles as supercapacitor electrode, J. Energy Storage 32 (2020), 101671.
[36] W. Lu, D. Sun, H. Yu, Synthesis and magnetic properties of size-controlled CoNi alloy nanoparticles, J. Alloy. Compd. 546 (2013) 229–233.
[37] Y. Liu, H. Yang, G. Tan, S. Miyazaki, B. Jiang, Y. Liu, Stress-induced FCC ↔ HCP martensitic transformation in CoNi, J. Alloy. Compd. 368 (2004) 157–163.
[38] N.V. Myung, K. Nobe, Electrodeposited iron group thin-film alloys: structure-property relationships, J. Electrochem. Soc. 148 (2001) C136.
[39] G. Krexner, J. Pleschiutschnig, G. Ernst, C. Hitzenberger, H.P. Karnthaler, A. Korner, O. Blaschko, Coherent modulated structure during the martensitic hcp-fcc phase transition in Co and in a CoNi alloy, Phys. Rev. Lett. 60 (1988) 2800–2803.
[40] Z. Boukha, A. Choya, M. Cortés-Reyes, B. de Rivas, L.J. Alemany, J.R. González-Velasco, J.I. Gutiérrez-Ortiz, R. López-Fonseca, Influence of the calcination temperature on the activity of hydroxyapatite-supported palladium catalyst in the methane oxidation reaction, Appl. Catal. B 277 (2020), 119280.
[41] M. Sudhakar, V.V. Kumar, G. Naresh, M.L. Kantam, S.K. Bhargava, A. Venugopal, Vapor phase hydrogenation of aqueous levulinic acid over hydroxyapatite supported metal (M = Pd, Pt, Ru, Cu, Ni) catalysts, Appl. Catal. B 180 (2016) 113–120.
[42] Z. Boukha, J.R. González-Velasco, M.A. Gutiérrez-Ortiz, Platinum supported on lanthana-modified hydroxyapatite samples for realistic WGS conditions: on the nature of the active species, kinetic aspects and the resistance to shut-down/start-up cycles, Appl. Catal. B 270 (2020), 118851.
[43] Q. Wang, X. Weng, B. Zhou, S. Lv, S. Miao, D. Zhang, Y. Han, S.L. Scott, F. Schüth, A. Lu, Selective production of aromatic alcohols from ethanol using a tailored bifunctional cobalt–hydroxyapatite catalyst, ACS Catal. 9 (2019) 7204–7216.
[44] H. Yan, H. Qin, W. Liang, X. Jin, Y. Zhang, X. Feng, Y. Liu, X. Chen, C. Yang, Enhanced performance of bimetallic PtCo/MCM-41 catalysts for glycerol oxidation in base-free medium, Catal. Sci. Technol. 9 (2019) 4909–4919.
[45] H. Yan, S. Yao, B. Yin, W. Liang, X. Jin, X. Feng, Y. Liu, X. Chen, C. Yang, Synergistic effects of bimetallic PtRu/MCM-41 nanocatalysts for glycerol oxidation in base-free medium: structure and electronic coupling dependent activity, Appl. Catal. B 259 (2019), 118070.
[46] L. Chen, W. Liu, H. Feng, Y. Ren, C. Chen, S. Wang, P. Yin, Y. Yang, X. Zhang, M. Wei, Oxygen binding energy of doped metal: a shortcut to efficient Ni-based bimetallic catalysts for the hydrodeoxygenation reaction, Catal. Sci. Technol. 11 (2021) 4376–4386.
[47] V.O.O. Gonçalves, W.H.S.M. Talon, V. Kartnaller, F. Venancio, J. Cajaiba, T. Cabioc, H. Clacens J., F. Richard, Hydrodeoxygenation of m-cresol as a depolymerized lignin probe molecule: synergistic effect of NiCo supported alloys, Catal. Today (2020).
[48] L. Zhao, X. Mu, T. Liu, K. Fang, Bimetallic Ni–Co catalysts supported on Mn–Al oxide for selective catalytic CO hydrogenation to higher alcohols, Catal. Sci. Technol. 8 (2018) 2066–2076.
[49] J.L.C. Fajín, M.N.D.S. Cordeiro, Light alcohols reforming towards renewable hydrogen production on multicomponent catalysts, Renew. Sustain. Energy Rev. 138 (2021), 110523.
[50] M. Chen, D. Liang, Y. Wang, C. Wang, Z. Tang, C. Li, J. Hu, W. Cheng, Z. Yang, H. Zhang, J. Wang, Hydrogen production by ethanol steam reforming over M-Ni/sepiolite (M = La, Mg or Ca) catalysts, Int. J. Hydrog. Energy 46 (2021) 21796–21811.
[51] K. Wang, X. Huang, Y. Liu, W. Fei, Z. Gu, Different morphologies of SiO2@Mg-Al-LDH nanocomposites as catalyst for the synthesis of propylene glycol methyl ether, J. Nanopart. Res. 22 (22) (2020) 1–14.
[52] Z. Zhang, Y. Zhu, H. Asakura, B. Zhang, J. Zhang, M. Zhou, Y. Han, T. Tanaka, A. Wang, T. Zhang, N. Yan, Thermally stable single atom Pt/m-Al2O3 for selective hydrogenation and CO oxidation, Nat. Commun. 8 (2017) 16100.
[53] P. Yang, J. Pan, Y. Liu, X. Zhang, J. Feng, S. Hong, D. Li, Insight into the role of unsaturated coordination O2c-Ti5c-O2c sites on selective glycerol oxidation over AuPt/TiO2 catalysts, ACS Catal. 9 (2018) 188–199.
[54] K. Coenen, F. Gallucci, B. Mezari, E. Hensen, M. van Sint Annaland, An in-situ IR study on the adsorption of CO_2 and H2O on hydrotalcites, J. CO2 Util. 24 (2018) 228–239.
[55] J. Yu, S.S.C. Chuang, The structure of adsorbed species on immobilized amines in CO_2 capture: an in situ IR study, Energy Fuel 30 (2016) 7579–7587.
[56] D. Miao, A. Goldbach, H. Xu, Platinum/apatite water-gas shift catalysts, ACS Catal. 6 (2016) 775–783.
[57] Z. Boukha, J. González-Prior, B.D. Rivas, J.R. González-Velasco, R. López-Fonseca, J.I. Gutiérrez-Ortiz, Synthesis, characterisation and behaviour of Co/hydroxyapatite catalysts in the oxidation of 1,2-dichloroethane, Appl. Catal. B 190 (2016) 125–136.
[58] J. Zhang, C. Zhao, A new approach for bio-jet fuel generation from palm oil and limonene in the absence of hydrogen, Chem. Commun. 51 (2015) 17249–17252.
[59] H. Chen, S. Yao, W. Lin, Z. Zhang, X. Hu, X. Liu, B. Yan, K. Chen, Y. Qin, Y. Zhu, X. Lu, P. Ouyang, J. Fu, J.G. Chen, Highly efficient conversion of oleic acid to heptadecane without external hydrogen source over atomic layer deposited bimetallic NiPt catalysts, Chem. Eng. J. 390 (2020), 124603.
[60] D. Han, W. Yin, S. Wang, S. Xia, Fabrication of a NiFe alloy oxide catalyst via surface reconstruction for selective hydrodeoxygenation of fatty acid to fatty alcohol, ACS Sustain. Chem. Eng. 9 (2021) 15027–15041.
[61] X. Kong, Z. Fang, X. Bao, Z. Wang, S. Mao, Y. Wang, Efficient hydrogenation of stearic acid over carbon coated Ni Fe catalyst, J. Catal. 367 (2018) 139–149.